Functionalized MoS_2-nanosheets for targeted drug delivery and chemo-photothermal therapy

Xueyi Zhang[a,1], Jianrong Wu[a,1], Gareth R. Williams[b*], Shiwei Niu[a], Qianqian Qian[a], Li-Min Zhu[a,*]

[a]College of Chemistry, Chemical Engineering and Biotechnology, Donghua University，Shanghai, 201620, China

[b]UCL School of Pharmacy, 29-39 Brunswick Square, London, WC1N 1AX, UK

[1] These authors contributed equally.

* Corresponding authors.

E-mail: lzhu@dhu.edu.cn (L.-M. Zhu) , Tel：+862167792655 (L.-M. Zhu); g.williams@ucl.ac.uk (G.R. Williams), +44 (0) 2077535868 (G.R. Williams)

Abstract

Molybdenum disulfide (MoS_2) has been extensively for biomedical applications due to itsexcellent photothermal conversion ability. In this paper, we reported a nanoplatform based on folic acid (FA) targeted dual-stimuli responsive MoS_2 nanosheets (FA-BSA-PEI-LA-MoS_2-LA-PEG, FBPMP) and explore this for the treatment of FA-receptor positive human breast cancer. The nanocomposites had a uniform diameter (133 nm), and could be loaded with the anti-cancer drug doxorubicin (DOX) to a high capacity (151.4 mg/g). The release of DOX was greatly accelerated at pH 5.0 as compared to pH 7.4. In addition, it was found that drug release is enhanced under the near infrared laser (NIR) irradiation, showing that the composites can be used as dual responsive systems, with DOX release controllable through pH or NIR irradiation. MTT assays and confocal experiments showed that FBPMP nanoplatform could selectively target and kill FA-positive MDA-MB-231 cells (a human breast cancer cell line). The platform also allowed the combination of chemotherapy and photothermal therapy, which led to synergistic effects superior to either monotherapy. The functionalized MoS_2 nanoplatform developed in this work hence could be a potent system for targeted drug delivery and synergistic chemo-photothermal cancer therapy.

Keywords: MoS_2; drug delivery; targeted; synergistic chemo-photothermal therapy

1. Introduction

Transition-metal dichalcogenides (TMDCs) are a family of two-dimensional layered materials with interesting physical, electronic and chemical properties [1]. The atoms in the layers are held together with strong covalent interactions, and the layers stack through van der Waals forces [2, 3]. TMDCs have been widely explored in energy storage, sensors, catalysis, and biomedicine [4-8]. In particular, the chalcogenides MoS_2, WS_2 and WSe_2 have been shown to be less toxic than graphene, suggesting they might have a wide range of biomedical applications [9]. MoS_2 has been explored as a drug

delivery carrier in a number of studies [10-12]. Notably, it has been proposed for use in photothermal therapy (PTT) treatments for cancer, because of its high photothermal conversion efficiency in the near-infrared (NIR) region [13, 14]. However, for clinical applications MoS_2 needs to be modified to improve its biocompatibility and colloidal stability [15, 16]; poly(ethylene glycol) [17, 18], peptides, silica and proteins [15, 19, 20] have all been used to this end. Despite those pioneering studies, research using MoS_2 for targeted drug delivery is still limited. PTT is a minimally invasive treatment, usually delivered using a NIR which can penetrate deep into tissue with minimal damage to healthy cells [21-23].

PTT can be combined with chemotherapy to deliver improved therapeutic performance in the treatment of cancer, has and such combined therapies have attracted increasing attention in recent years [24-29]. They can most potently be delivered through responsive drug delivery systems (DDSs) [30-36], which respond to stimuli such as light, magnetic fields, or ultrasonication [37-39], or to changes in redox potential, pH and the presence of absence of particular molecules [40-43].

The blood and tissue of the human body have a roughly neutral pH, while tumors are weakly acidic: this difference can be exploited in pH-targeted drug delivery. However, most DDSs enter cells through the endocytic pathway. The pH of the endosomes in which they are first taken into the cell also have a pH of about 5.0 [44]. This means that if a pH-responsive system is designed to retain its drug cargo at neutral pH but release it at pH 5.0, it is vital to ensure that the DDS escapes from the endosome in order to deliver its active ingredient payload to the cytoplasm. If the DDS does not escape from the endosomes, the drug will be released inside them, reducing the therapeutic efficacy [45]. Thus, it is of great importance that we endow the DDS with the ability to access the cytoplasm [46-48].

In this work, we constructed a smart DDS based on MoS_2 functionalized with folicacid grafted bovine serum albumin (FA-BSA) to permit targeting to human breast cancer cells and improve the stealthiness of the nanocarriers under physiological conditions (Scheme 1)[49-51]. Additional modification with poly(ethylene glycol) to enhance dispersibility and stability. The materials were fully characterized, and their drug release profiles, *in vitro* cytotoxicity and cellular uptake explored. This nanoplatform could be a promising therapeutic agent and smart carrier for the synergistic combination of phototherapy towards biomedical applications.

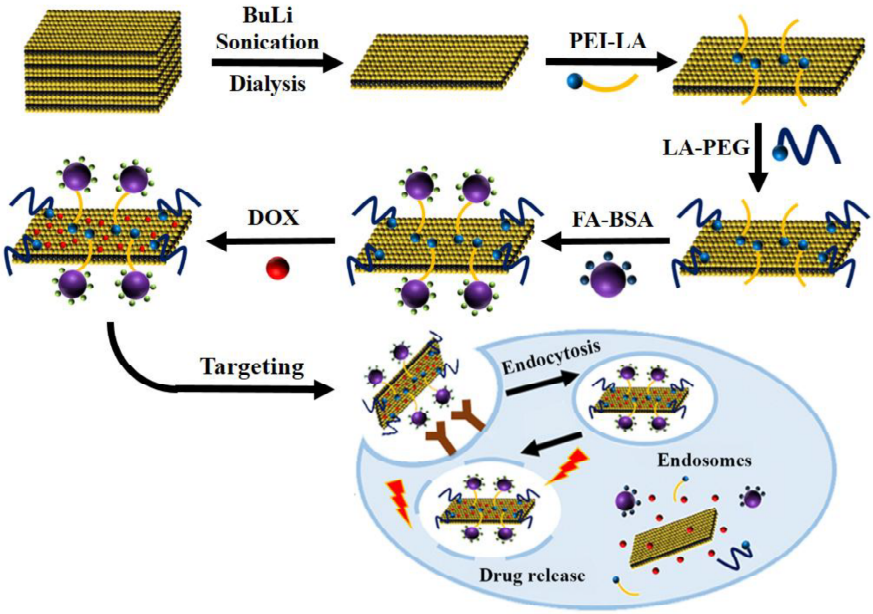

Scheme 1. Schematic illustration for the construction of MoS_2-based nanocomposites for synergistic chemo-photothermal therapy.

2 Materials and methods

2.1 Materials

Poly(ethylene imine) (PEI, M_w = 25 kDa), poly(ethylene glycol) (PEG, M_w = 2 kDa), doxorubicin (DOX), N-hydroxysuccinimide (NHS), N-[3-(dimethylamino)propyl]-N'-ethyl-carbodiimide hydrochloride (EDC), bovine serum albumin (BSA), alpha-lipoic acid (LA), folic acid (FA), and n-BuLi solution in hexane (2.4 M), N,N′-Dicyclohexylcarbodiimide (DCC), Triethylamine (TEA) were all purchased from Aladdin Biochemical Polytron Technologies Inc. 2-morpholine sulfonic acid (MES) was obtained from Shanghai Titan Polytron Technologies Inc. Acetonitrile was sourced from Shanghai Ling Feng Chemical reagents Co., Ltd, and dimethyl sulfoxide (DMSO) from the Shanghai Pumai Biotechnology Co., Ltd. 3-(4,5-dimethyl-thiazol-yl)-2,5-diphenyltetrazolium bromide (MTT), MoS_2 powder (2–8 μm, 99%) and phosphate buffered saline (PBS) were purchased from Sigma–Aldrich. 4′-6-diamidino-2-phenylindole (DAPI) was procured from Nanjing Keygen Biotech. MDA-MB-231 cells and L929 cells were purchased from the Type Culture Collection of the Chinese Academy of Sciences. All other materials and dialysis bags were obtained from the Sinopharm Chemical Reagent Co., Ltd. Analytical grade chemicals were used throughout. Milli-Q water with resistance18.2 MΩ cm was employed for all experiments requiring water.

2.2 Preparation of MoS_2 nanosheets

MoS_2 was exfoliated following a previously reported protocol [52]. In brief, MoS_2 flakes (2 g) were stirred with a solution of n-butyllithium in hexane (2 mL; 1.6 M) under an N_2 atmosphere for 48 h. The mixture was then washed with hexane to remove residual n-butyllithium, combined with 30 mL water, and ultrasonicated for 90 min to achieve effective exfoliation. Subsequently, it was centrifuged at 3000 rpm to separate the multilayered MoS_2 nanosheets. The exfoliated MoS_2 was dialyzed for 3 days against water using a cellulose membrane (MWCO: 10 kDa) to obtain the MoS_2 nanosheets.

2.3 Functionalization of few layers MoS_2

82.4 mg LA was first dissolved in 20 mL acetonitrile, then EDC (191.7 mg) and NHS (115.1 mg) were added under stirring. Afterwards the mixture was added to a PEI solution (300 mg in 20 mL water [pH 7.4]), and stirred overnight. The product, denoted LA-PEI, was obtained after dialyzing against water with a cellulose membrane (MWCO: 1 kDa) for 24h. 30 mg LA-PEI was added to dispersions of MoS_2 (0.25 mg/mL, 10 mL water) and then ultrasonicated for 30 min. After stirring overnight, the resultant product (PEI-LA-MoS_2) was dialyzed with water against a cellulose membrane (MWCO: 3.5 kDa).

Next, 45 mg LA and 300 mg PEG were dissolved in 2.4 mL of dichloromethane under stirring until the solution had clarified. 12 mg DCC and 7.2 μL TEA were then added, and the organic solvent was removed with a rotary evaporator to give LA-PEG, the pH adjusted to 8.0. PEI-LA-MoS_2 (0.5 mg/mL in water, 3 mL) was added to 15 mg LA-PEG. After ultrasonication for 30 min, the reaction was allowed to proceed for 12 h at room temperature to obtain PEI-LA-MoS_2-LA-PEG (PMP). The precipitate was suspended in water (50 mL) and centrifuged at 10,000 rpm three times to obtain a pure product.

2.4 Preparation of targeted nanocomposite

FA (3mg/mL) was dissolved in 3 mL of MES buffer solution (50 mM, pH=6.0), then reacted with EDC (3 mg) and NHS (3 mg) for 20 min in the dark. The resultant solution (0.5 mL) was then combined with 100 mL of a BSA solution in MES (0.4 mg/mL, 50 mM, pH=6.0) for 12h. After dialyzing against water with a cellulose membrane (MWCO: 5 kDa) for 24 h, FA-BSA was obtained. The FA–BSA solution (20 mL) was reacted with PMP (50mg) for 5 min, after which EDC (24 mg) and NHS (14 mg) were added and the mixture stirred for 12h. FA-BSA-PEI-LA-MoS_2-LA-PEG (FBPMP) was obtained after the mixed solution was centrifuged for 15 min at 5,000 rpm and dispersed in water

three times.

2.5 Drug loading

FBPMP and the model drug DOX were mixed in pure water in various ratios and stirred overnight to yield FBPMP(DOX). FBPMP interacted with DOX by electrostatic interaction. The supernatant was collected by centrifugation and the unloaded drug concentration was determined by UV-vis spectroscopy (UV3600, Shimadzu Corporation, Japan) at 480nm. Drug loading efficiency of FBPMP was calculated by use of the following equation:

$$\text{Drug loading efficiency of FBPMP (\%)} = \frac{\text{total weight of DOX-weight of unloaded DOX}}{\text{total weight of FBPMP}} \times 100\%$$

2.6 Materials characterization

The morphology of MoS_2 was measured using transmission electron microscopy (TEM; JEM-2100, JEOL, Japan). The thickness and size of the MoS_2 particles were determined with a 5500 atomic force microscope (AFM; Agilent, USA). The zeta potential was quantified with a ZS90 Zetasizer instrument (Malvern, UK). Dynamic light scattering (DLS) was performed with static light scattering instrument (BI-200SM, Brookhaven, USA).). ^1H NMR spectra were collected on a Bruker DRX 400 nuclear magnetic resonance spectrometer. X-ray diffraction (XRD) measurements were performed on a D8 Advance X-ray diffractometer equipped with Cu Kα radiation (λ=1.5418 Å) (Bruker, Switzerland). Fourier transform infrared (FT-IR) spectra were recorded on a Nicolet Nexus 870 spectrometer (Nicolet Instruments Inc. USA). UV-vis absorbance was measured by ultraviolet visible spectrophotometer (UV3600, Shimadzu Corporation, Japan). The chemical state of the MoS_2 nanosheets was confirmed by X-ray photoelectron spectroscopy (Escalab 250Xi, USA) analysis. The photothermal effect were analyzed using a laser device (Shanghai Xilong Optoelectronics Technology Co. Ltd., Shanghai, China) at a wavelength of 808 nm.

2.7 Photothermal effects

Various concentrations of the nanocomposites from 0.5 mg/mL to 1.5 mg/mL in PBS (pH 7.4) were irradiated with an 808 nm laser (0.5 W/cm^2) to measure the photothermal effects. The influence of the laser power density was ascertained by irradiating a suspension of FBPMP (0.5 mg/mL) under laser power densities from 0.5 W/cm^2 to 1.25 W/cm^2, and the thermal stability of the materials was determined by irradiating for 5 min (0.75 W/cm^2) over five on–off cycles. The temperature of the solution was monitored using a DT-8891E thermocouple linked to a digital thermometer (Shenzhen

Everbest Machinery Industry, Shenzhen, China). For the volume of solution was 1mL, the temperature of the solution could be determined to be homogeneous everywhere. Also, the photothermal conversion efficiency of FBPMP was calculated using the following equation:

$$\eta=\frac{hS(T_{max}-T_{am})-Q_0}{I(1-10^{-A})}$$

where h equals the heat transfer coefficient, S equals the surface area, T_{max} equals equilibrium temperature, T_{am} equals surrounding ambient temperature, Q_0 equals heat absorption of the quartz cell, I equals the laser power, A equals the absorbance of FBPMP at 808 nm.

2.8 *In vitro* drug release

A dispersion of FBPMP(DOX) in PBS (3 mL, pH 7.4 or pH 5.0) with a FBPMP concentration of 1 mg/mL was introduced into a dialysis bag (M_w = 6 KDa) and then dialyzed against different PBS solutions (50 mL) with exposure to 808 nm laser irradiation (1 W/cm^2) and shaking (200 rpm) for 5 min. A sample of media (1 mL) was withdrawn at periodic time intervals, and an equal volume of fresh buffer was added. The temperature was 37 °C throughout the experiment. The concentration of DOX released was determined by using UV–vis spectrophotometry (480 nm). The control group was treated under identical conditions but without irradiation. The cumulative amount of DOX released from the composites was calculated as follows:

$$\text{Cumulative release DOX (\%)}=\frac{\text{Total amount of DOX - Free DOX}}{\text{Total amount of DOX}}\times 100\%$$

2.9 Cell culture and cytotoxicity assays & *in vitro* combined therapies

The cytotoxicity of FBPMP(DOX) on the MDA-MB-231 cell line (FA receptor positive) was evaluated by using the MTT assay, with the L929 cell line (FA receptor negative) used as a control. Briefly, MDA-MB-231 and L929 cells were grown in DMEM cell culture medium supplemented with penicillin (100 U/mL) and streptomycin (100 U/mL). Confluent cells were then harvested and plated in 96-well plates at a density of 1 x 10^4 cells per well (200 μL of cell suspension per well). FBPMP(DOX) or the free drug (concentration range of 0.01 to 10 μg/mL) were added to each well, after 24 hours of culture, MTT reagent (10μL, 5 mg/mL) was added followed by incubation at 37 °C in a 5% CO_2 atmosphere for 4 h. The supernatant was then carefully removed. Aspirate and MTT-formazan produced by live cells is solubilized in 150 mL of DMSO for 20 minutes. Finally, the absorbance at 490 nm was measured using a microplate reader (MULTSIKAN MK3, ThermoFisher, USA). Cell viability (%) was determined from the absorbance at 450 nm and normalised to negative control wells

containing untreated cells. Experiments were performed in triplicate, 40 wells per experiment.

A second set of experiments was performed to assess the potential for photochemo therapies. MDA-MB-231 cells were cultured in a 96-well plate at 1×10^4 cells per well (200 μL) for 24h, then were co-cultured with FBPMP(DOX) or FBPMP. Cells were divided into six treatment groups with concentration range of 0.01 to 10 μg/mL as follows: 1 PBS; 2 NIR; 3 free DOX; 4 FBPMP; 5 FBPMP+NIR (photothermal therapy); 6 FBPMP(DOX) (chemotherapy); and 7 FBPMP(DOX)+NIR (synergistic therapy). After incubation for 12 h, the cells were washed with 100 μL PBS and 100 μL culture medium was then added to the wells. The cells were irradiated with a laser (808 nm, 0.5 W/cm^2) for 5 min in the case of groups 2, 5 and 7, before the cells were cultured for a further 24 h and an MTT assay used to measure cell viability.

2.10 *In vitro* cellular uptake

Cell targeting efficiency was investigated with confocal laser scanning microscopy (CLSM). Either MDA-MB-231 cells or L929 cells were seeded at a density of 1×10^5 cells per well (1mL) in 24-well plates and cultured for 24 h. The media was aspirated and 2 mL of fresh DMEM containing free DOX, FBPMP or FBPMP(DOX) was added (concentration range of 0.01 to 10 μg/mL). 3 h later, the medium was discarded, and the cells were washed three times with 1mL PBS (pH 7.4) for 15 min. Subsequently, the cells were fixed with chilled methanol (-20 °C) and stained with Hochest 33342 (1 μg/mL). The cells in all the groups were cultured for another 2 h and then washed and fixed with glutaraldehyde for 30 min. The cell nuclei were stained with DAPI and the fluorescent images of the cells were observed by CLSM (Nikon Eclipse Ti-S, Nikon Ltd, Japan).

2.11 Statistical analysis

One-way analysis of variance (ANOVA) statistical method was performed to evaluate the experimental data. All experiments were repeated at least three times, and the data are displayed as mean ± standard deviation (SD). Statistical significance was considered at $P < 0.05$ (*), $P < 0.01$ (**) and $P < 0.001$ (***).

3. Results and discussion

3.1 Synthesis and characterization of nanocomposites

The strategy underlying the construction of the FBPMP nanocomposites is illustrated in Scheme S1 (Supporting Information). MoS_2 nanosheets were obtained by the chemical exfoliation method

following a previously reported method [44]. As depicted in Scheme S1a and b, LA–PEI was synthesized by amide coupling and the MoS_2 nanosheets functionalized with LA-PEI using a thiol reaction. After mixing MoS_2–LA–PEI with LA-PEG, PEG was grafted on the surface of single-layered MoS_2 to form PMP (Scheme S1c). FA-BSA was synthesized by amide coupling and then coated on the surface of PMP to form the final product FBPMP (Scheme S1d and e).

The morphology of MoS_2 after BuLi treatment was characterized by TEM, which shows the material to consist of exfoliated sheets (Fig. 1a). XPS data (Fig. 1b) show characteristic peaks at 517 eV (Mo 3s), 413 eV (Mo 3p1), 359 eV (Mo 3p3), 233eV (Mo 3d,) 64 eV (Mo 4s) and 38 eV (Mo 4p). These results are consistent with the literature for MoS_2 [53]. The AFM images in In Fig.1c and Fig. 1d, show that the thickness of the MoS_2 nanosheets were approximately 1.3 nm, which indicates they comprise around 7 to 10 layers [52]. As shown in Fig. S1, diffraction peaks in the XRD patterns can be indexed to MoS_2 (JCPDS10-0319).

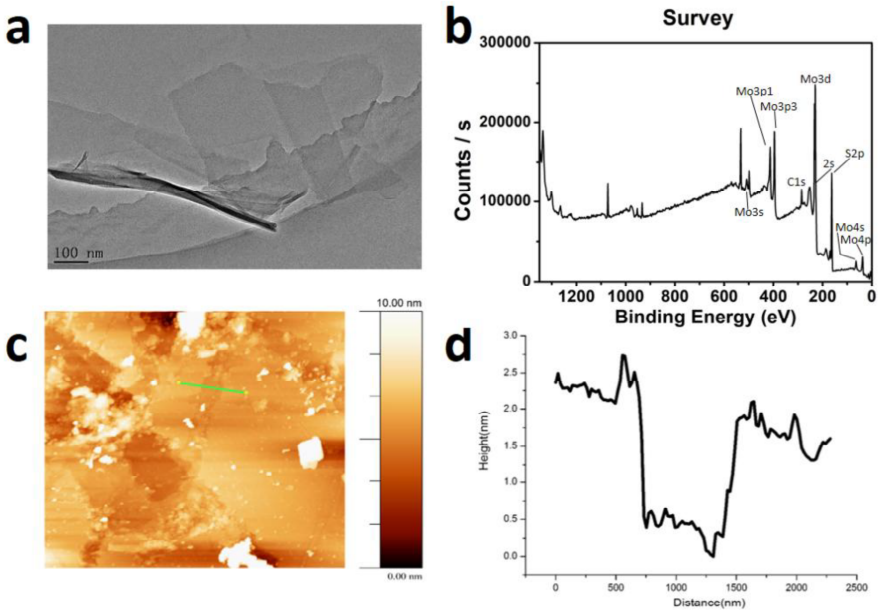

Fig. 1. Structural characterization of the exfoliated MoS_2 sheets. (a) TEM image; (b) XPS survey data; (c) an AFM image; (d) the corresponding AFM height profile.

In order to confirm the successful synthesis of LA-PEI and FA-BSA, ^{1}H-NMR spectra were performed. The spectrum of LA-PEI (Fig. S2, Table S1) displayed peaks from the CH_2 groups of the lipoic acid at δ = 7.71 - 7.88 ppm and 2.72 ppm. Resonances from the NH_2 and NH groups of PEI can be seen at δ = 2.99 - 3.25 ppm; the peak of hydrogen on alkyl of the lipoic acid at δ=2.37-2.59ppm. These results are consistent with the successful synthesis of PEI-LA. The ^{1}H-NMR spectrum of FA-BSA displayed peaks from the BSA amino acids at δ = 3.78 ppm (Fig. S3, Table S1), from the alkyl

groups of folic acid at δ = 3.18 ppm, and the amine groups of FA at δ = 3.00 ppm, these results well illustrate the successful synthesis of FA-BSA.

UV–vis spectroscopy further validated the successful synthesis of FA-BSA (Fig. 2a). FA exhibits adsorption peaks at 278 nm and 363 nm, which are also evident in the spectrum of FA-BSA. The successful synthesis of PEI-LA-MoS_2 and FBPMP was confirmed by FT-IR spectroscopy. The IR spectrum of PEI-LA-MoS_2 is given in Fig. 2b, and shows characteristic peaks at 3436 cm^{-1} and 1638 cm^{-1}. These demonstrate the presence of amide groups on PEI-LA-MoS_2, indicating that LA and PEI are connected successfully through the amide bond. The IR spectrum of PEI-LA-MoS_2-LA-PEG is also given in Fig. 2b. Bands at 1648 cm^{-1} and 1562 cm^{-1} corresponded to the amide bands of -CONH- groups in the PEG, proving the successfully synthesis of PMP. Additional distinctive peaks are observed in the spectrum of FBPMP (Fig. 2b). These arise at 1461 cm^{-1} indicate the stretching vibrations of BSA, while characteristic peaks at 1193 cm^{-1}, 1115 cm^{-1} and 1049 cm^{-1} indicated the existence of PEG and FA. These results further verified that the FBPMP was successfully prepared.

The hydrodynamic diameters of the nanocomposites were quantified by DLS, and the results are shown in Fig. 2c. The hydrodynamic diameters of the nanocomposites are about 133 nm, which is appropriate for use as cell-targeted drug delivery system [54]. Zeta potentials were measured to investigate the surface charge of the nanocomposites (Fig. 2d). The MoS_2 nanosheets exhibited a zeta potential of −38.3 mV, which changed to 19.8 mV on coating with LA-PEI. The zeta potential changed from negative to positive because of the presence of amino groups in PEI, further confirming the successful grafting of LA-PEI. The zeta potential of FA-BSA was −4.3 mV due to the carboxyl groups on FA. After BSA–FA grafting, the zeta potential of the FBPMP was 5.4 mV, which again illustrated the success of the modification process.

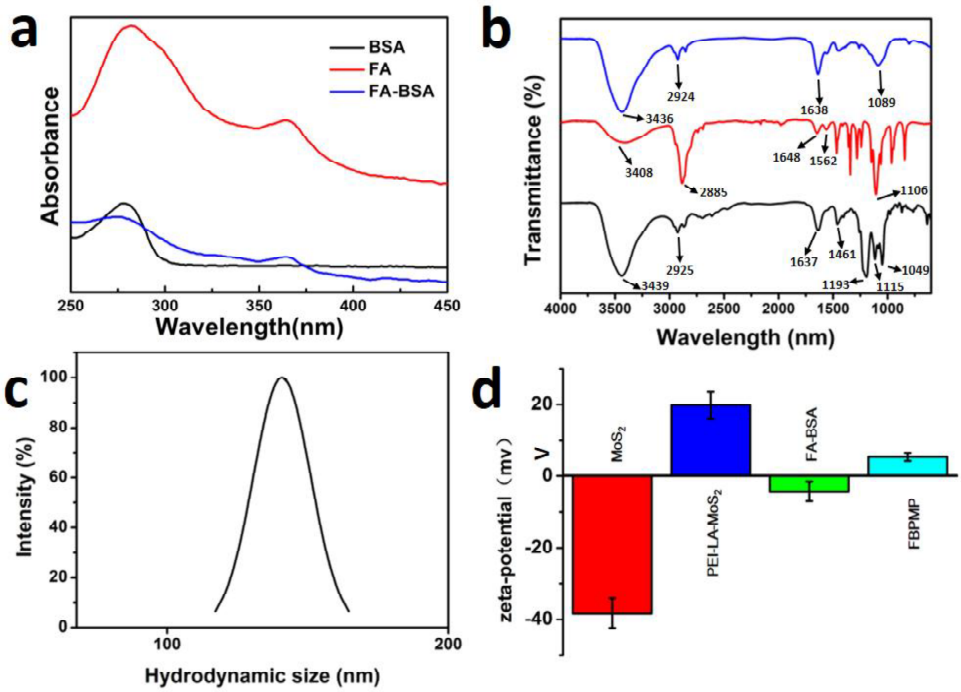

Fig. 2. (a)UV–Vis absorption spectra of BSA, FA, and FA-BSA ; (b) FT-IR spectra of PEI-LA-MoS_2 (blue), PMP (red) and FBPMP (black); (c) DLS data on FBPMP; (d) the zeta potentials of the nanocomposites at various stages of functionalization. Data are presented as mean ± SD (n=3).

3.2 Photothermal activity

It is well known that MoS_2 nanocomposites have good photothermal conversion efficiency, the photothermal activity of FBPMP was tested as follows. In Fig. 3a, the photothermal heating effect of a 0.5 mg/mL suspension of the FBPMP composite under irradiation by different laser-powers is depicted. When the laser power was 0.75 W/cm^2 the temperature reached to 63.1 °C within 300 seconds. A laser power intensity dependent photothermal effect was observed, as would be expected. The photothermal effect is also found to be concentration-dependent under irradiation at 0.5 W/cm^2 (Fig. 3b). These results indicate the suitability of FBPMP for photothermal therapy and potentiality for thermal ablation of tumors. After five on-off cycles of irradiation (Fig. 3c), the temperature response of the FBPMP suspension remains largely constant. This suggests that FBPMP has excellent photothermal stability [55]. Meanwhile, the photothermal conversion efficiency of FBPMP was calculated to be 54.2%.

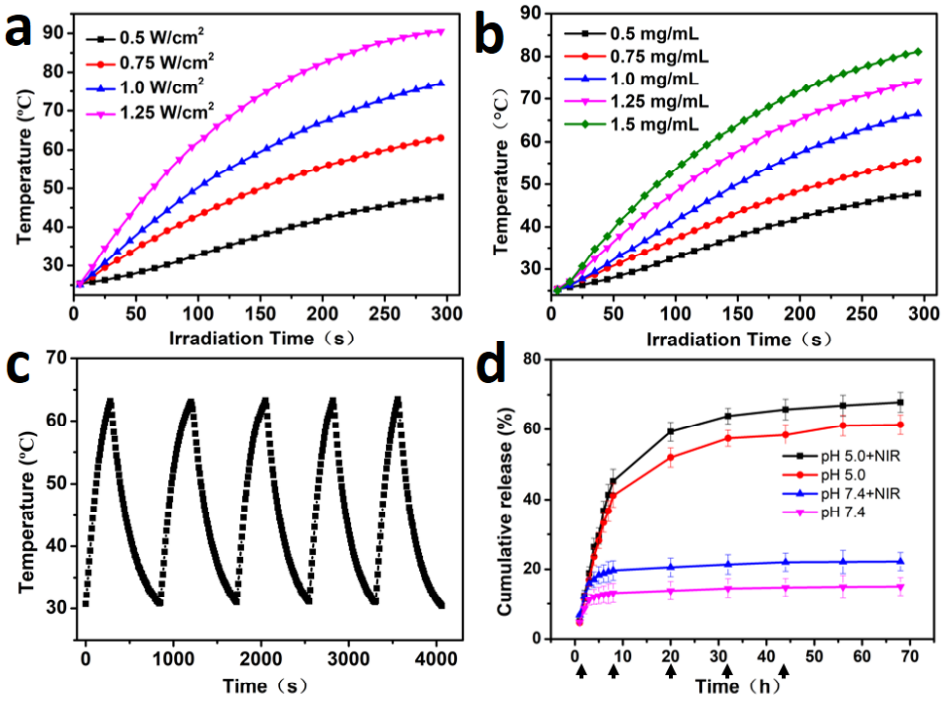

Fig. 3. (a) Heating curves of FBPMP at the fixed concentration of 0.5 mg/mL under different laser power densities; (b) Heating curves of different concentrations FBPMP under laser power densities at 0.5 W/cm^2; (c) A plot showing the response of FBPMP over five on–off cycles (0.5 mg/mL suspension, 0.75 W/cm^2 laser density); (d) DOX release profiles of FBPMP(DOX) at different pHs with and without 808 nm laser irradiation (0.5 W/cm^2), the arrow means the laser irradiation. Data are presented as mean ± SD (n=3).

3.3 *In vitro* drug release

When the ratio of FBPMP and DOX was 2:1 by mass, the drug loading efficiency was the optimal and 1g FBPMP was able to load 151.4 mg DOX (Table S2). The *in vitro* release behavior of FBPMP(DOX) was investigated in different pH media (5.0 and 7.4) with and without laser irradiation (Fig. 3d). The release of DOX was faster and reached a greater extent at pH 5.0. For example, the cumulative release of DOX after 68 hours at pH 5.0 (61.3 %) was much greater than that at pH 7.4 (15.0 %). This phenomenon can be attributed to a reduction of the hydrophobic interactions between FBPMP and DOX at low pH [56]. Since tumors are more acidic than normal tissues, and the endosomal environment is even more acidic with a pH of about 5.0, this should be beneficial for tumor treatments [57]. At a given pH, there is greater DOX release with laser irradiation than without. This indicates that NIR light-triggered photothermal heating could promote the release of DOX and

accelerate the death of cancerous cells.

3.4 In vitro cell viability

The synergistic therapeutic efficacy of the FBPMP(DOX) (concentration range of 0.01 to 10 μg/mL) against cancer cells were investigated by MTT assay after incubation with both MDA-MB-231 cells and L929 cells (Fig. 4), groups treated with NIR were irradiated with a laser (808 nm, 0.5 W/cm^2) for 5 min. The cell viability of FBPMP-treated cells was above 80% in all cases, showing the composite to have high biocompatibility even at high concentrations of 10 μg/mL. NIR irradiation alone was found to have no effect on cell viability: both L929 cells and MDA-MB-231 cells showed essentially identical cell viabilities (> 90%) whether they were treated with laser irradiation or not (Fig. S4). When the cell viabilities in an equivalent dose of DOX, FBPMP(DOX) groups were lower than FBPMP groups, indicating the chemotherapy effect of the MoS_2 nanocomposites. On the other hand, the cell viabilities in FBPMP with laser irradiation groups were lower than FBPMP groups, too, indicated the PTT effect of the MoS_2 nanocomposites. The viability of free DOX incubated cells was higher than FBPMP(DOX) incubated MDA-MB-231 cells with laser irradiation at various of concentrations. But the most important thing is the cell viabilities in the synergistic therapy group were much lower than in the monotherapy groups (chemotherapy or PTT). The results demonstrated that the MoS_2 nanocomposites can kill cancer cells through the synergistic therapy. It is worth noting that NIR laser irradiation both induces heat for photothermal therapy as well as accelerating the release of DOX from FBPMP(DOX) through heat stimulated dissociation of the π–π stacking interactions between DOX and FBPMP [49]. This leads to enhanced chemotherapy. And the cytotoxic effect of FBPMP(DOX) with or without laser irradiation was intensely enhanced in MDA-MB-231 cells compared with L929 cells. All these results confirmed that the constructed multifunctional drug delivery system was effective to kill the tumor cells and was promising in chemo-photothermal combined cancer therapy.

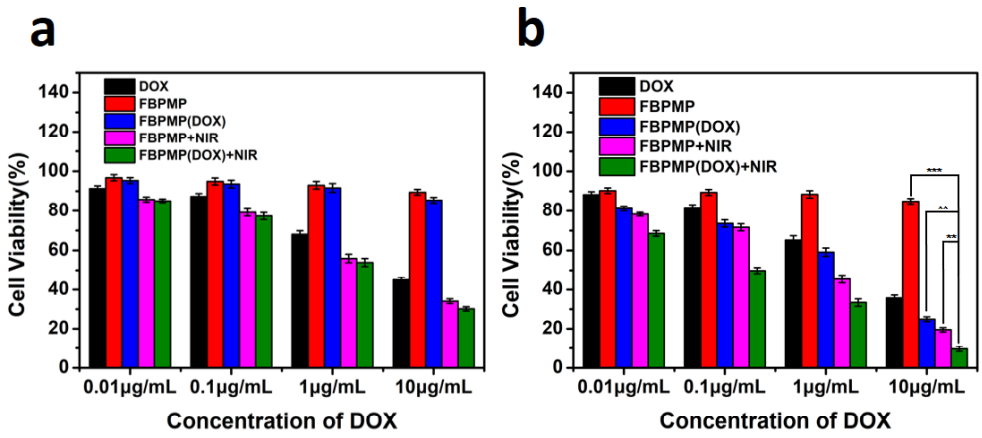

Fig. 4. The viability of (a) L929 cells and (b) MDA-MB-231 cells exposed to different concentrations of DOX or DOX-loaded nanocomposites, with or without laser irradiation. Data are presented as mean ± SD (n=3). Statistical significance: $P < 0.01$ (**) and $P < 0.001$ (***).

3.5 Cellular uptake

The targeting ability of the nanocomposites was investigated by CLSM. MDA-MB-231 cells and L929 cells, which are respectively FA-receptor positive and FA-receptor negative, were cultured with FBPMP(DOX), PMP(DOX) or free DOX. Both cell types could take up FBPMP(DOX) and PMP(DOX), as shown by the coincident presence of DAPI (blue) and DOX (red) fluorescence (Fig. 5). Relatively little free DOX is taken up by either cell line, but more DOX fluorescence is evident in the case of the MDA-MB-231 cells. MDA-MB-231 cells incubated with FBPMP(DOX) exhibited much greater DOX fluorescence than those exposed to PMP(DOX) (without the FA-BSA group). This demonstrates that the cellular uptake of FBPMP(DOX) by MDA-MB-231 cells involves FA receptor-mediated endocytosis. In contrast, the uptake of FBPMP(DOX) and PMP(DOX) by L929 cells was similar, and the DOX fluorescence was weak. This arises because of the lack of an FA receptor on the L929 cells. Therefore, we concluded that nanocomposites modified with FA-BSA chould efficiently delivery DOX into MDA-MB-231 cells which is beneficial for chemo-photothermal combined cancer therapy and the cellular uptake of the nanocomposites might be *via* the FA-receptor-mediated endocytosis process.

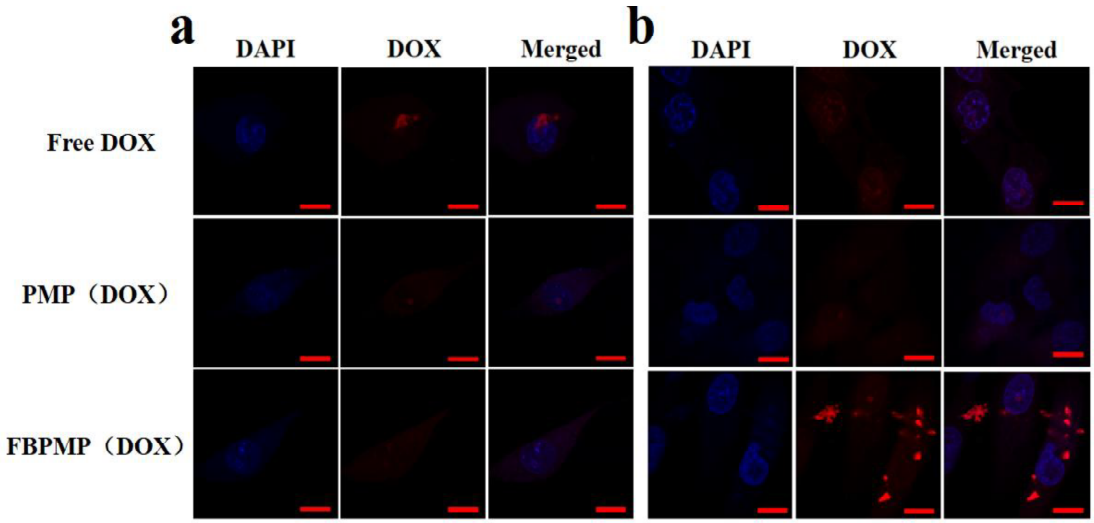

Fig. 5. Confocal microscope images of (a) L929 and (b) MDA-MB-231 cells incubated with DOX, PMP(DOX) or FBPMP(DOX) at an equivalent DOX concentration of 5.0 μg/mL for 4 h. The bar represents 25 μm.

4. Conclusion

A multifunctional MoS_2-based drug delivery system (FBPMP) was successfully synthesized in this work and shown to allow tumor-targeting synergistic chemo-photothermal therapy. MoS_2 nanosheets were modified with the targeting moiety FA-BSA to improve the stealthiness of the nanocarriers under physiological conditions and PEG was added to achieve excellent biocompatibility. The nanocomposite had a uniform diameter (133 nm), and could be loaded with the anti-cancer drug DOX to a high loading capacity of 151.4 mg DOX / g FBPMP. The release of DOX is faster in lower pH (5.0) environments than at the physiological pH, which is promising for tumour-specific delivery. Release is also accelerated under near infrared light irradiation. The nanocomposites can be specifically delivered into cancerous (MDA-MB-231) cells *via* a receptor-mediated endocytosis pathway using folic acid targeting, the cell viabilities in the synergistic therapy group were much lower than in the monotherapy groups (chemotherapy or PTT), and the nanocomposites were found to be able to induce the death of cancerous cells while leaving healthy cells unaffected.

Acknowledgements

This research was financially supported by the Shanghai Municipal Science and Technology Commission Project 16410723700, the Biomedical Textile Materials "111 Project" of the China

Ministry of Education (No B07024) and the UK-China Joint Laboratory for Therapeutic Textiles (based at Donghua University). The authors further thank the UCL Global Engagement Fund for their kind support.

References

[1] Q.H. Wang, K. Kalantarzadeh, A. Kis, J.N. Coleman, M.S. Strano, Electronics and optoelectronics of two-dimensional transition metal dichalcogenides, Nat Nanotechnol, 7 (2012) 699-712.

[2] M. Chhowalla, H.S. Shin, G. Eda, L.J. Li, K.P. Loh, H. Zhang, The chemistry of two-dimensional layered transition metal dichalcogenide nanosheets, Nat Chem, 5 (2013) 263-275.

[3] D. Voiry, A. Mohite, M. Chhowalla, ChemInform abstract: phase engineering of transition metal dichalcogenides, Chem Soc Rev, 44 (2015) 2702-2712.

[4] K. Kalantar-Zadeh, J.Z. Ou, T. Daeneke, M.S. Strano, M. Pumera, S.L. Gras, Two-dimensional transition metal dichalcogenides in biosystems, Adv Funct Mater, 25 (2015) 5086-5099.

[5] W. Yin, X. Dong, Y. Jie, J. Pan, Z. Yao, Z. Gu, Y. Zhao, MoS_2-nanosheet-assisted coordination of metal Ions with porphyrin for rapid detection and removal of cadmium Ions in aqueous media, Acs Appl Mater Inter, 9 (2017) 21362-21370.

[6] Y. Chen, Y. Wu, B. Sun, S. Liu, H. Liu, Two-dimensional nanomaterials for cancer nanotheranostics, Small, 13 (2017).

[7] J.X. Song, X.Y. Tang, D.M. Zhou, W. Zhang, T.D. James, X.P. He, H. Tian, Fluorogenic 2D glycosheet for the simultaneous identification of human and avian-receptor specificity in influenza viruses, Mater Horiz, 4 (2017) 431-436.

[8] M. Wahiba, X.Q. Feng, Y. Zang, T. James, J. Li, G.R. Chen, X.P. He, A supramolecular pyrenyl glycoside-coated 2D MoS_2 composite electrode for selective cell capture, Chem Commun, 52 (2016) 11689-11692.

[9] W.Z. Teo, E.L. Chng, Z. Sofer, M. Pumera, Cytotoxicity of exfoliated transition-metal dichalcogenides (MoS_2 , WS_2 , and WSe_2) is lower than that of graphene and its analogues, Chem, 20 (2014) 9627.

[10] A. Zhang, A. Li, W. Tian, Z. Li, C. Wei, Y. Sun, W. Zhao, M. Liu, J. Liu, A target-directed

chemo-photothermal system based on transferrin and copolymer-modified MoS_2 nanoplates with pH-activated drug release, Chem-Eur J, 23 (2017) 11346.

[11] T. Liu, C. Wang, X. Gu, H. Gong, L. Cheng, X. Shi, L. Feng, B. Sun, Z. Liu, Drug delivery with PEGylated MoS_2 nano-sheets for combined photothermal and chemotherapy of cancer, Adv Mater, 26 (2014) 3433-3440.

[12] R. Deng, H. Yi, Y. Fang, L. Fu, Y. Zeng, Y. Wang, Y. Li, Y. Liu, S. Ji, Y. Su, Facile exfoliation of MoS_2 nanosheets by protein as a photothermal-triggered drug delivery system for synergistic tumor therapy, RSC Adv, 6 (2016) 77083-77092.

[13] M. Zhou, R. Zhang, M. Huang, W. Lu, S. Song, M.P. Melancon, M. Tian, D. Liang, C. Li, A chelator-free multifunctional [64Cu]CuS nanoparticle platform for simultaneous micro-PET/CT imaging and photothermal ablation therapy, J Am Chem Soc, 132 (2010) 15351.

[14] J. Mou, C. Yu, M. Ming, K. Zhang, C. Wei, H. Chen, J. Shi, Facile synthesis of liposome/$Cu_{2-x}S$-based nanocomposite for multimodal imaging and photothermal therapy, Sci China Mater, 58 (2015) 294-301.

[15] J. Lee, J. Kim, W.J. Kim, Photothermally controllable cytosolic drug delivery based on core-shell MoS_2-porous silica nanoplates, Chem of Mater, 28 (2016) 6417-6424.

[16] H. Deng, X. Yang, Z. Gao, MoS_2 nanosheets as an effective fluorescence quencher for DNA methyltransferase activity detection, Analyst, 140 (2015) 3210-3215.

[17] T. Liu, C. Wang, W. Cui, H. Gong, C. Liang, X. Shi, Z. Li, B. Sun, Z. Liu, Combined photothermal and photodynamic therapy delivered by PEGylated MoS_2 nanosheets, Nanoscale, 6 (2014) 11219-11225.

[18] S.S. Chou, M. De, J. Kim, S. Byun, C. Dykstra, Y. Jin, J. Huang, V.P. Dravid, Ligand conjugation of chemically exfoliated MoS_2, J Am Chem Soc, 135 (2013) 4584.

[19] S. Ariyasu, J. Mu, X. Zhang, Y. Huang, E.K. Yeow, H. Zhang, B. Xing, Investigation of thermally induced cellular ablation and heat response triggered by planar MoS_2-based nanocomposite, Bioconjugate Chem, 28 (2017) 1059-1067.

[20] S. Wang, L. Tan, P. Liang, T. Liu, J. Wang, C. Fu, J. Yu, J. Dou, H. Li, X. Meng, Layered MoS_2 nanoflowers for microwave thermal therapy, J Mater Chem B, 4 (2016) 2133-2141.

[21] V. Shanmugam, S. Selvakumar, C.S. Yeh, ChemInform abstract: near-Infrared light-responsive nanomaterials in cancer therapeutics, Chem Soc Rev, 43 (2014) 6254-6287.

[22] J.T. Robinson, S.M. Tabakman, Y. Liang, H. Wang, H.S. Casalongue, D. Vinh, H. Dai, Ultrasmall reduced graphene oxide with high near-infrared absorbance for photothermal therapy, J Am Chem Soc, 133 (2011) 6825-6831.

[23] Y. Zhang, C.Y. Ang, Y. Zhao, Polymeric nanocarriers incorporating near-infrared absorbing agents for potent photothermal therapy of cancer, Polym J, 48 (2015) 589–603.

[24] L. Chen, W. Feng, X. Zhou, K. Qiu, Y. Miao, Q. Zhang, M. Qin, L. Li, Y. Zhang, C. He, Facile synthesis of novel albumin-functionalized flower-like MoS_2 nanoparticles for in vitro chemo-photothermal synergistic therapy, Rsc Adv, 6 (2016) 13040-13049.

[25] X. Meng, Z. Liu, Y. Cao, W. Dai, K. Zhang, H. Dong, X. Feng, X. Zhang, Cancer Therapy: Fabricating aptamer-conjugated PEGylated-MoS_2/Cu1.8S theranostic nanoplatform for multiplexed imaging diagnosis and chemo-photothermal therapy of cancer, Adv Funct Mater, 27 (2017) 1605592.

[26] J. Liu, A. Zhang, A. Li, W. Tian, Z. Li, W. Chen, S. Yong, Z. Wei, M. Liu, A target-directed chemo-photothermal system based on transferrin and copolymer modified MoS_2 nanoplates with pH-activated drug release, Chem-Eur J, 23 (2017) 11346.

[27] Y. Fei, W. Duan, Y. Li, W. Hao, Y. Zhou, P. Min, H. Liu, L. Xin, H. Zheng, NIR-laser-controlled drug release from DOX/IR-780-loaded temperature-sensitive-liposomes for chemo-photothermal synergistic tumor therapy, Theranostics, 6 (2016) 2337-2351.

[28] T. Bao, W. Yin, X. Zheng, X. Zhang, J. Yu, X. Dong, Y. Yong, F. Gao, L. Yan, Z. Gu, One-pot synthesis of PEGylated plasmonic MoO(3-x) hollow nanospheres for photoacoustic imaging guided chemo-photothermal combinational therapy of cancer, Biomaterials, 76 (2016) 11-24.

[29] X. Zhu, Y. Zhang, H. Huang, H. Zhang, L. Hou, Z. Zhang, Functionalized graphene oxide-based thermosensitive hydrogel for near-infrared chemo-photothermal therapy on tumor, J Biomater Appl, 30 (2016) 480-481.

[30] X. Yao, X. Niu, K. Ma, P. Huang, J. Grothe, S. Kaskel, Y. Zhu, Graphene quantum dots-capped magnetic mesoporous silica nanoparticles as a multifunctional platform for controlled drug delivery, magnetic hyperthermia, and photothermal therapy, Small, 13 (2017) 1602225.

[31] S. Yu, X. Zhang, G. Tan, L. Tian, D. Liu, Y. Liu, X. Yang, W. Pan, A novel pH-induced thermosensitive hydrogel composed of carboxymethyl chitosan and poloxamer cross-linked by glutaraldehyde for ophthalmic drug delivery, Carbohydr Polym, 155 (2017) 208-217.

[32] X. Li, L. Xing, Y. Hu, Z. Xiong, R. Wang, X. Xu, L. Du, M. Shen, X. Shi, An RGD-modified hollow silica@Au core/shell nanoplatform for tumor combination therapy, Acta Biomater, 62 (2017).

[33] L. Kong, L. Xing, B. Zhou, L. Du, X. Shi, Dendrimer-Modified MoS_2 Nanoflakes as a Platform for Combinational Gene Silencing and Photothermal Therapy of Tumors, ACS Appl. Mater. Interfaces, 9 (2017) 15995-16005.

[34] D. Li, Y. Zhang, S. Wen, Y. Song, Y. Tang, X. Zhu, M. Shen, S. Mignani, J.P. Majoral, Q. Zhao, Construction of polydopamine-coated gold nanostars for CT imaging and enhanced photothermal therapy of tumors: an innovative theranostic strategy, J. Mater. Chem. B, 4 (2016) 4216-4226.

[35] J. Li, Y. Hu, J. Yang, P. Wei, W. Sun, M. Shen, G. Zhang, X. Shi, Hyaluronic acid-modified Fe_3O_4@Au core/shell nanostars for multimodal imaging and photothermal therapy of tumors, Biomaterials, 38 (2015) 10-21.

[36] P. Wei, J. Chen, Y. Hu, X. Li, H. Wang, M. Shen, X. Shi, Dendrimer-Stabilized Gold Nanostars as a Multifunctional Theranostic Nanoplatform for CT Imaging, Photothermal Therapy, and Gene Silencing of Tumors, Adv. Healthcare Mater, 5 (2016) 3203-3213.

[37] Y. Matsushita-Ishiodori, T. Ohtsuki, Photoinduced RNA interference, Acc Chem Res, 45 (2012) 1039-1047.

[38] R. Namgung, K. Singha, M.K. Yu, S. Jon, Y.S. Kim, Y. Ahn, I.K. Park, W.J. Kim, Hybrid superparamagnetic iron oxide nanoparticle-branched polyethylenimine magnetoplexes for gene transfection of vascular endothelial cells, Biomaterials, 31 (2010) 4204-4213.

[39] R. Deckers, C.T. Moonen, Ultrasound triggered, image guided, local drug delivery, J Control Release, 148 (2010) 25-33.

[40] S. Son, N. Ran, J. Kim, K. Singha, W.J. Kim, Bioreducible polymers for gene silencing and delivery, Acc Chem Res, 45 (2012) 1100-1112.

[41] S. Son, J. Nam, J. Kim, S. Kim, W.J. Kim, i-motif-driven Au nanomachines in programmed siRNA delivery for gene-silencing and photothermal ablation, Acs Nano, 8 (2014) 5574-5584.

[42] R. Mo, T. Jiang, R. Disanto, W. Tai, Z. Gu, ATP-triggered anticancer drug delivery, Nat Commun, 5 (2014) 3364.

[43] B.R. Twaites, C.D.L.H. Alarcón, D. Cunliffe, M. Lavigne, S. Pennadam, J.R. Smith, D.C.

Górecki, C. Alexander, Thermo and pH responsive polymers as gene delivery vectors: effect of polymer architecture on DNA complexation in vitro, J Control Release, 97 (2004) 551.

[44] K. Sakai-Kato, N. Nishiyama, M. Kozaki, T. Nakanishi, Y. Matsuda, M. Hirano, H. Hanada, S. Hisada, H. Onodera, H. Harashima, General considerations regarding the in vitro and in vivo properties of block copolymer micelle products and their evaluation, J Control Release, 210 (2015) 76-83.

[45] J. Kim, H. Kim, W.J. Kim, Single-layered MoS_2-PEI-PEG nanocomposite-mediated gene delivery controlled by photo and redox stimuli, Small, 12 (2016) 1184-1192.

[46] X. Liu, P. Zhang, W. Rödl, K. Maier, U. Lächelt, E. Wagner, Toward artificial immunotoxins: traceless reversible conjugation of RNase a with receptor targeting and endosomal escape domains, Mol Pharm, 14 (2016) 1439-1449.

[47] Z.Y. Ong, C. Yang, W. Cheng, Z.X. Voo, W. Chin, J.L. Hedrick, Y.Y. Yang, Biodegradable cationic poly(carbonates): Effect of varying side chain hydrophobicity on key aspects of gene transfection, Acta Biomater, 54 (2017) 201-211.

[48] K. Sudo, K. Niikura, K. Iwaki, S. Kohyama, K. Fujiwara, N. Doi, Human-derived fusogenic peptides for the intracellular delivery of proteins, J Control Release, 255 (2017) 1-11.

[49] A. Topete, M. Alatorre-Meda, P. Iglesias, E.M. Villar-Alvarez, S. Barbosa, J.A. Costoya, P. Taboada, V. Mosquera, Fluorescent drug-loaded, polymeric-based, branched gold nanoshells for localized multimodal therapy and imaging of tumoral cells, Acs Nano, 8 (2014) 2725-2738.

[50] M.S. Strozyk, M. Chanana, I. Pastoriza-Santos, J. Pérez-Juste, L.M. Liz-Marzán, Stimuli-Responsive Materials: Protein/Polymer-Based Dual-Responsive Gold Nanoparticles with pH-Dependent Thermal Sensitivity (Adv. Funct. Mater. 7/2012), Adv Funct Mater, 22 (2012) 1322-1322.

[51] L. Han, Y. Zhang, X. Chen, Y. Shu, J.H. Wang, Protein-modified hollow copper sulfide nanoparticles carrying indocyanine green for photothermal and photodynamic therapy, J Mater Chem B, 4 (2015) 105-112.

[52] J. Wu, D.H. Bremner, S. Niu, H. Wu, J. Wu, H. Wang, H. Li, L.M. Zhu, Functionalized MoS_2 nanosheet-capped periodic mesoporous organosilicas as a multifunctional platform for synergistic targeted chemo-photothermal therapy, Chem Eng J, 342 (2018) 90-102.

[53] X. Yang, W. Fu, W. Liu, J. Hong, Y. Cai, C. Jin, M. Xu, H. Wang, D. Yang, H. Chen,

Engineering crystalline structures of two-dimensional MoS_2 sheets for high-performance organic solar cells, J Mater Chem A, 2 (2014) 7727-7733.

[54] D.R. Elias, A. Poloukhtine, V. Popik, A. Tsourkas, Effect of ligand density, receptor density, and nanoparticle size on cell targeting, Nanomed-Nanotechnol, 9 (2013) 194.

[55] Q. Zou, M. Abbas, L. Zhao, S. Li, G. Shen, X. Yan, Biological photothermal nanodots based on self-assembly of peptide-porphyrin conjugates for antitumor therapy, J Am Chem Soc, 139 (2017) 1921-1927.

[56] J. Zhu, L. Liao, X. Bian, J. Kong, P. Yang, B. Liu, pH-controlled delivery of doxorubicin to cancer cells, based on small mesoporous carbon nanospheres, Small, 8 (2012) 2715-2720.

[57] Y. Wang, K. Wang, J. Zhao, X. Liu, J. Bu, X. Yan, R. Huang, Multifunctional mesoporous silica-coated graphene nanosheet used for chemo-photothermal synergistic targeted therapy of glioma, J Am Chem Soc, 135 (2013) 4799-4804.